Supplementary information: The role of pressure and defects in the wurtzite to rock salt transition in cadmium selenide

Anders Lervik,*,† Ingeborg-Helene Svenum,‡ Zhaohui Wang,¶ Raffaela Cabriolu,†,§ Enrico Riccardi,‖ Stefan Andersson,¶ and Titus S. van Erp†

†*Department of Chemistry, Norwegian University of Science and Technology, Høgskoleringen 5, 7491 Trondheim, Norway*

‡*Department of Materials and Nanotechnology, SINTEF Industry, P.O. Box 4760 Torgarden, 7465 Trondheim, Norway*

¶*Department of Metal Production and Processing, SINTEF Industry, P.O. Box 4760 Torgarden, 7465 Trondheim, Norway*

§*Department of Physics, Norwegian University of Science and Technology, Høgskoleringen 5, 7491 Trondheim, Norway*

‖*Department of Informatics, UiO, Gaustadalléen 23B, 0373 Oslo, Norway.*

* E-mail: anders.lervik@ntnu.no

Equilibrium results and comparison with DFT

We show the radial distribution functions for Cd–Se in figure S1 and the MD results from investigating the pressure region for the stability of the honeycomb structure in figure S2. From these brute-force MD simulations, we find that the 5-coordinated structure is (meta)stable up to approximately 5.3 GPa. We have compared the stability of the structures (wurtzite,

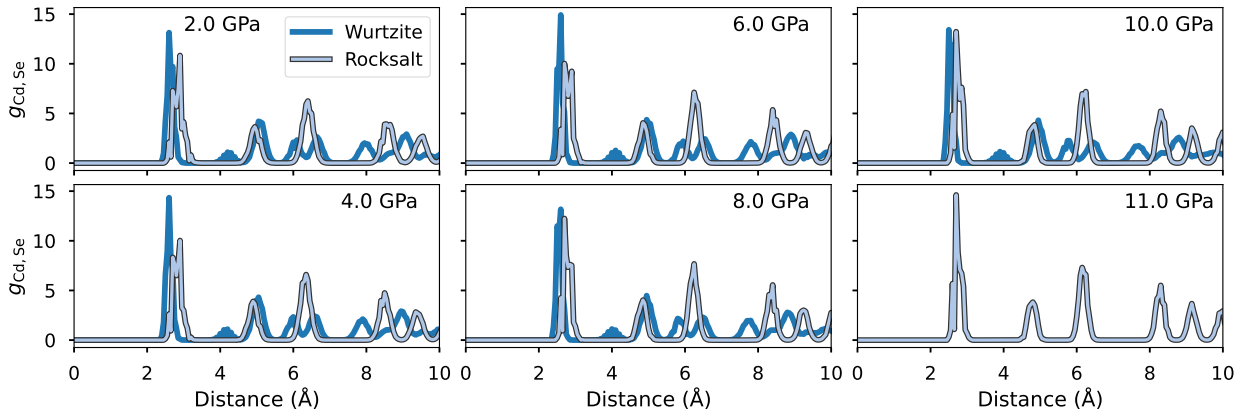

Figure S1 Radial distribution functions for Cd and Se atoms ($g_{\mathrm{Cd,Se}}$) at the different pressures.

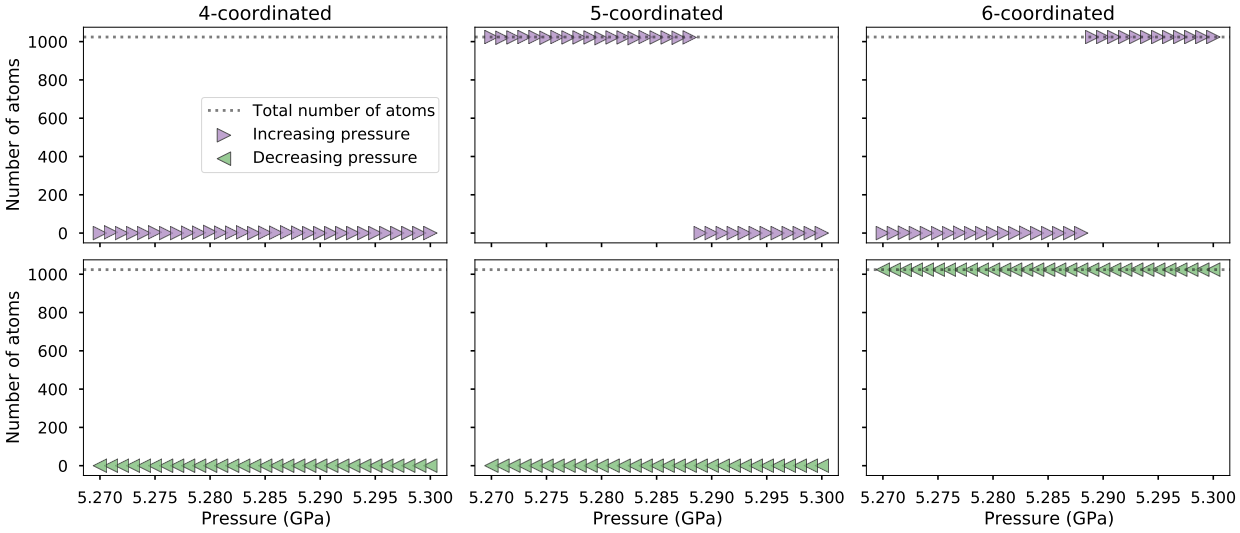

Figure S2 (Upper row) Final coordination numbers (purple right triangles) for MD simulations starting from a honeycomb structure at different pressures. The pressure (starting at 5.27 GPa) was increased in a step-wise fashion in increments of 1 MPa. Each pressure was simulated for 10 ns. We have also investigated the final coordination number when decreasing the pressure (lower row, green left triangles). In this case, the initial configuration was the final structure (a rock-salt conformation) obtained from the simulations where the pressure was increased.

rock salt, and honeycomb) with the classical force field[1] and density functional theory (DFT). CdSe supercells for the wurtzite ($P6_3mc$), rock salt ($Fm\bar{3}m$) and a honeycomb structure ($P6_3/mmc$) consisting of 1024 atoms were optimized using DFT calculations as implemented by the Vienna Ab initio Simulation Package (VASP).[2,3] The structures were adapted from Materials Project[4] (wurtzite and rock salt) and Shimojo et al.[5] (honeycomb). The generalized-gradient approximation (GGA) with the Perdew–Burke-Ernzerhof (PBE) exchange-correlation functional[6] was applied. The cutoff energy for the plane waves was set to 550 eV, and a single Γ-centered kpoint was used. The structures were relaxed until the forces on the atoms were below 0.01 eV/Å. The energy relative to the wurtzite structure calculated by DFT was compared with calculations on the same structures with the classical force field (see Table S1). For the classical force field, the potential energy was minimized using the steepest descent algorithm as implemented in GROMACS. Structure optimization included the size and shape of the simulation cell in the DFT calculations. The GROMACS optimization involved both using the cell volume obtained by DFT as well as manual optimization of the cell size (with re-optimization of the atomic coordinates). Results for the force field using both cell sizes are reported in Table S1 but the results with optimized volume should be considered most relevant for the discussion of the quality of the classical force field. Enthalpy change as a function of pressure was taken into account in an approximate manner by adding a $P\Delta V$ term to the energies where the volume change (ΔV) was calculated for the zero pressure structures, i.e., the pressure was not explicitly introduced in the optimization. DFT and force field results agree qualitatively on the relative stability of the three phases at zero pressure and both predict a phase transition pressure between 2 and 4 GPa for the wurtzite-rock salt transition. At pressures above 6 GPa, rock salt was predicted to be significantly more stable than the other two phases. The force field predicted the honeycomb structure to be roughly equally stable as wurtzite around 6 GPa (and somewhat more stable at higher pressures). DFT also predicted that the honeycomb structure becomes more stable relative to wurtzite with increasing pressure but that wurtzite remains the more

stable phase up to 10 GPa.

Table S1 Energies (per CdSe pair) of the different phases obtained with DFT and the classical force field. The enthalpy changes in pressurized materials are approximated by adding a $P\Delta V$ term only taking the volume change (ΔV) between the zero pressure structures into account. For the force field results are reported both for cell volumes equal to the ones optimized with DFT as well as those optimized with the force field itself (see text for details).

		Relative enthalpy (eV)					
		Pressure (GPa)					
Method	Structure	0	2	4	6	8	10
DFT	wurtzite	0.00	0.00	0.00	0.00	0.00	0.00
	rock salt	0.29	0.14	-0.02	-0.17	-0.33	-0.48
	honeycomb	0.21	0.17	0.14	0.10	0.07	0.03
force field	wurtzite	0.00	0.00	0.00	0.00	0.00	0.00
w. DFT vol.	rock salt	0.13	-0.02	-0.17	-0.33	-0.48	-0.64
	honeycomb	0.09	0.05	0.01	-0.02	-0.06	-0.09
force field	wurtzite	0.00	0.00	0.00	0.00	0.00	0.00
w. opt. vol.	rock salt	0.14	0.02	-0.11	-0.24	-0.37	-0.49
	honeycomb	0.09	0.06	0.04	0.01	-0.02	-0.05

We also compared defect energies from DFT simulations with the classical force field (see Table S2). The defect energy (E_{defect}) of a system with n pairs of CdSe atoms removed, was defined as,

$$E_{\mathrm{defect}} = \frac{E_{\mathrm{system}} - (E_{\mathrm{bulk}} - nE_{\mathrm{CdSe}})}{n} \tag{1}$$

where E_{system} is the energy of the system with defects, E_{bulk} is the energy of the system without defects, and E_{CdSe} is the energy of the system without defects, per Cd–Se pair in the system. Defects were created in the wurtzite structure either by removing one pair of neighboring Cd–Se atoms, or by removing a pair of Cd–Se atoms separated by a larger (> 10 Å) distance. The defect energies were calculated both with DFT and with the classical force field for the same structures.

Table S2 Defect energies obtained with DFT and the classical force field. The relative difference was calculated as the difference between the classical and the DFT defect energy, divided by the DFT defect energy. The P1/P2-configurations are structures where one Cd–Se pair (neighboring atoms) has been removed. The F1/F2-configurations are structures where the Cd–Se atoms removed were separated by a larger distance. The P16-configuration is a case with 16 neighboring Cd–Se pairs removed.

	Energy (eV)		Relative
Configuration	DFT	Classical	difference
F1	2.95	3.49	0.18
F2	3.16	3.73	0.18
P1	1.93	2.31	0.20
P2	1.92	2.24	0.17
P16	1.22	1.88	0.54

Additional results for the RETIS simulations (without defects)

The positions used for the different RETIS simulations are given in table S3. Additional results for the Steinhardt order parameters for trajectories generated with the RETIS algorithm are shown in figures S3–S5. The change in volume and coordination numbers for 9 additional trajectories (at pressures 2, 4, and 6 GPa) are shown in figures S6 and S7, with corresponding Steinhardt order parameters in figures S8–S10.

Table S3 Position of interfaces used in the RETIS simulations.

Pressure (GPa)	**Position of interfaces** ($Å^3$)
2	-28.15, -28.05, -27.90, -27.80, -27.60, -27.50, -27.40, -27.30, -27.20, -27.10, -27.00, -26.90, -26.80, -26.70, -26.60, -26.50, -26.40, -26.30, -26.20, -26.10, -26.00, -25.90, -25.80, -25.65, -25.45, -25.25, -25.05, -24.80, -24.40, -24.00
4	-27.18, -27.10, -27.00, -26.90, -26.80, -26.70, -26.60, -26.50, -26.40, -26.30, -26.20, -26.10, -26.00, -25.90, -25.80, -25.65, -25.45, -25.25, -25.05, -24.80, -24.40, -24.00
6	-26.40, -26.30, -26.20, -26.10, -26.00, -25.90, -25.80, -25.85, -25.75, -25.65, -25.60, -25.50, -25.40, -25.30, -25.10, -24.90, -24.70, -24.40, -24.00
6*	-26.84, -26.82, -26.70, -26.65, -26.60, -26.50, -26.45, -26.40, -26.20, -26.00, -25.00, -24.80
8	-25.75, -25.70, -25.60, -25.50, -25.40, -25.30, -25.20, -25.10, -25.00, -24.90, -24.80, -24.60, -24.40, -24.00
10	-25.20, -25.10, -24.90, -24.80, -24.70, -24.60, -24.50, -24.40, -24.20, -24.00

* Random removal (16 Cd, 16 Se)

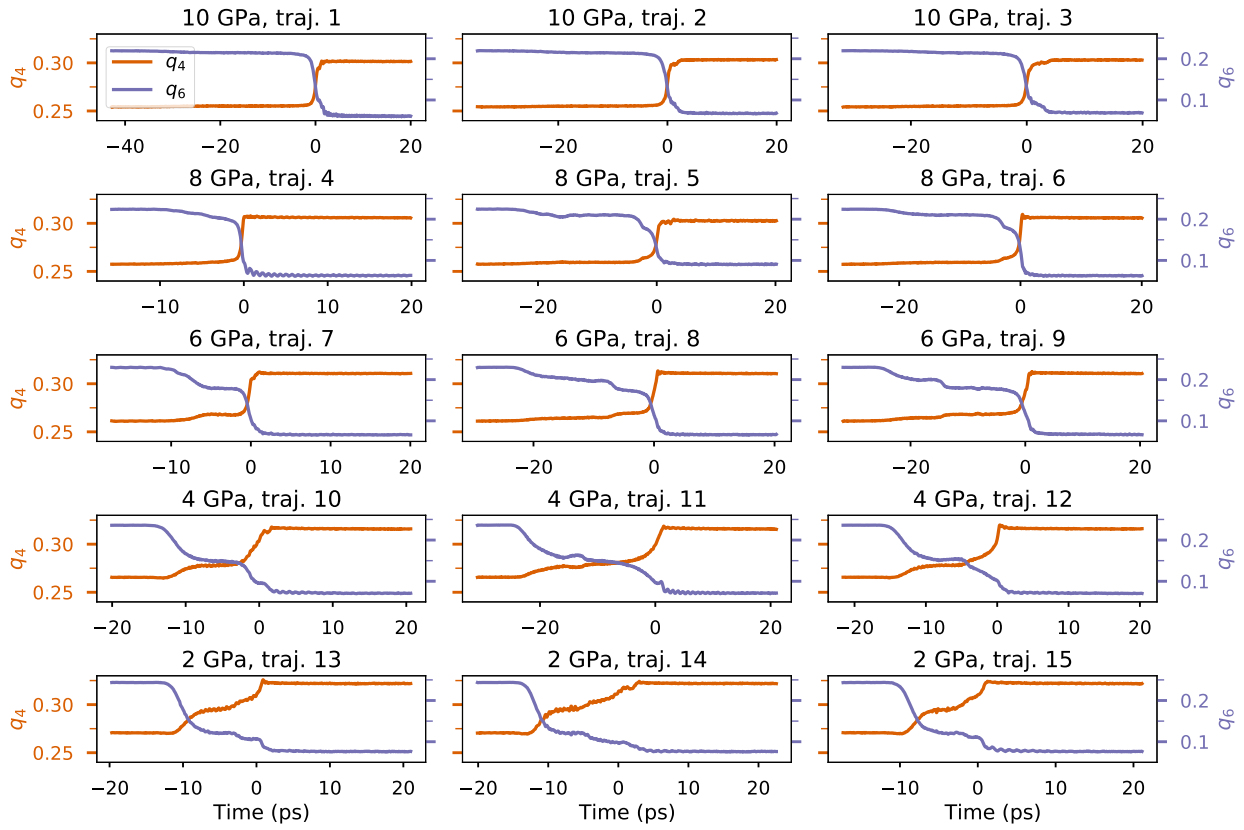

Figure S3 Mean Steinhardt order parameters of order 4 (q_4) and 6 (q_6) for representative trajectories at the considered pressures. These trajectories are the same as shown in figure 3 in the main article, and the time has been shifted identically.

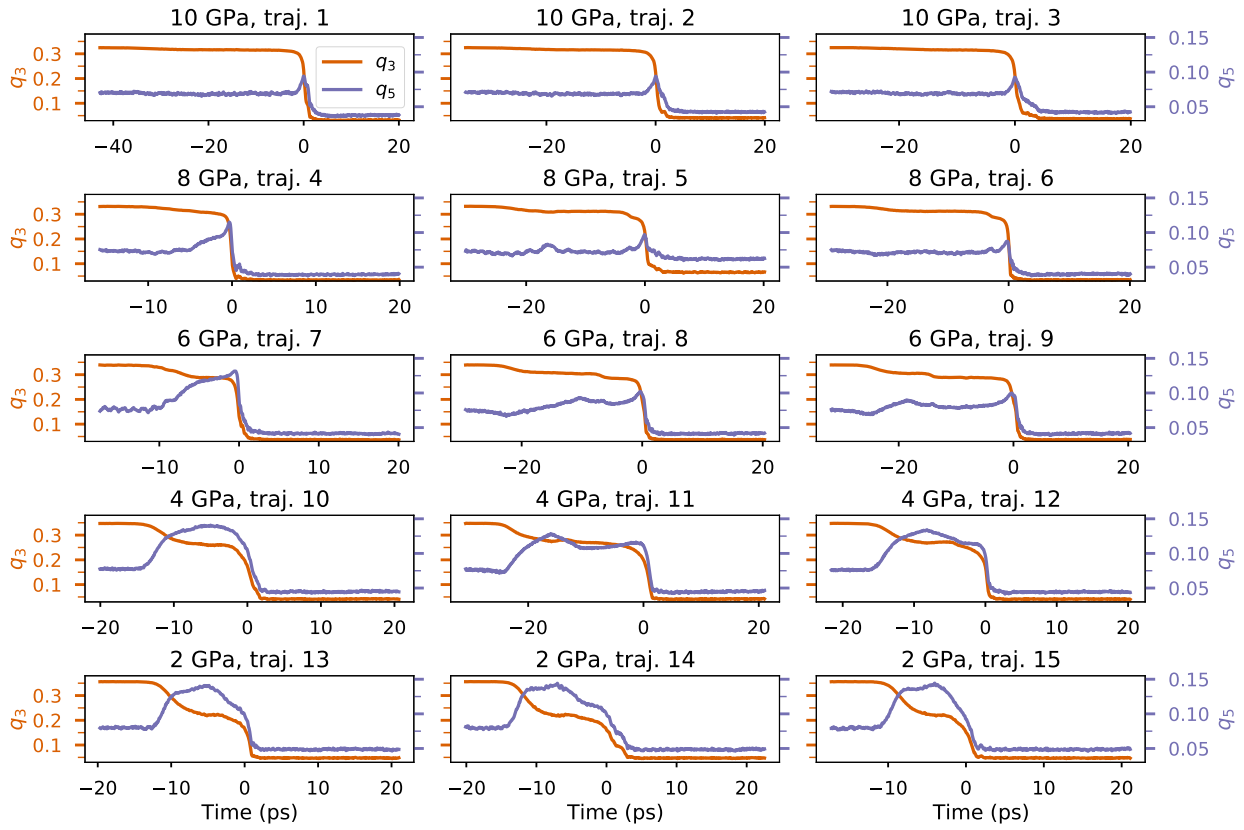

Figure S4 Mean Steinhardt order parameters of order 3 (q_3) and 5 (q_5) for representative trajectories at the considered pressures. These trajectories are the same as shown in figure 3 in the main article, and the time has been shifted identically.

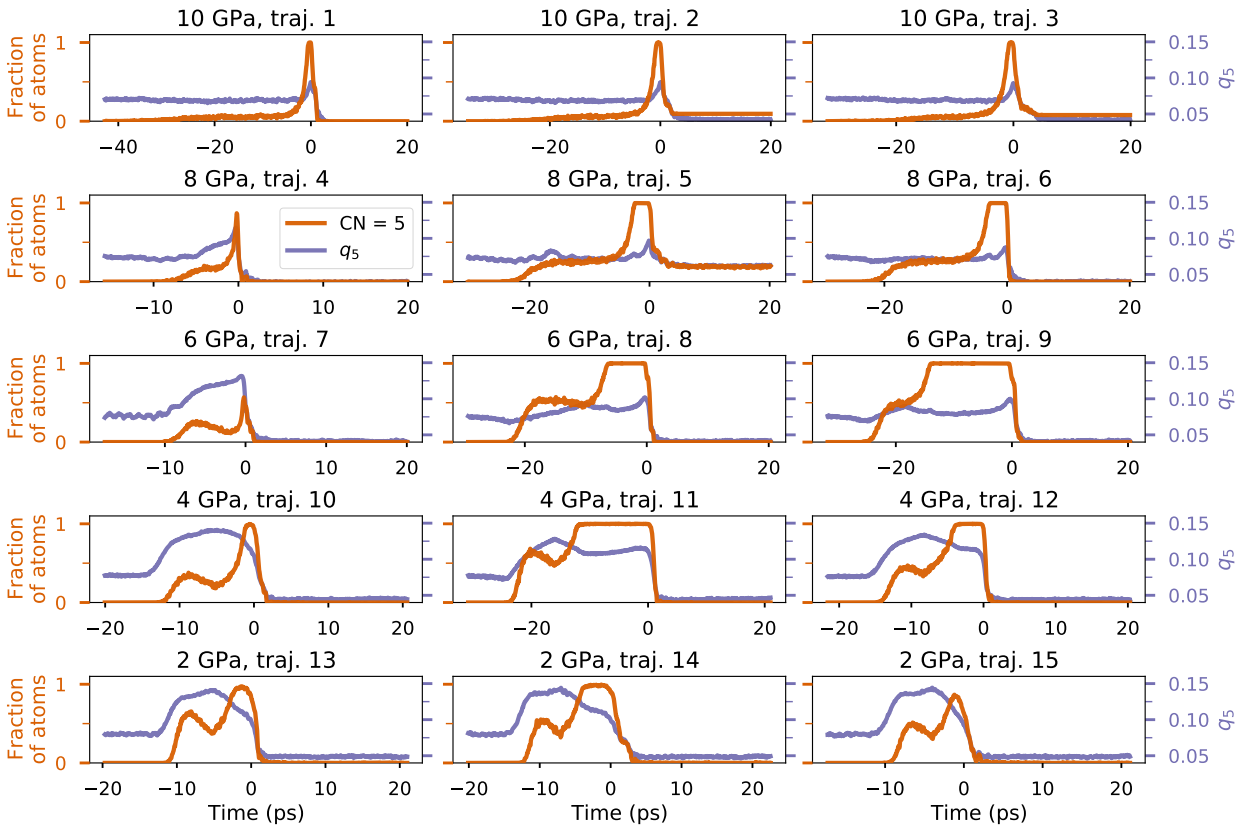

Figure S5 Fraction of atoms assigned as 5-coordinated ("CN = 5") and the mean Steinhardt order parameter of order 5 (q_5) for representative trajectories at the considered pressures. These trajectories are the same as shown in figure 3 in the main article, and the time has been shifted identically.

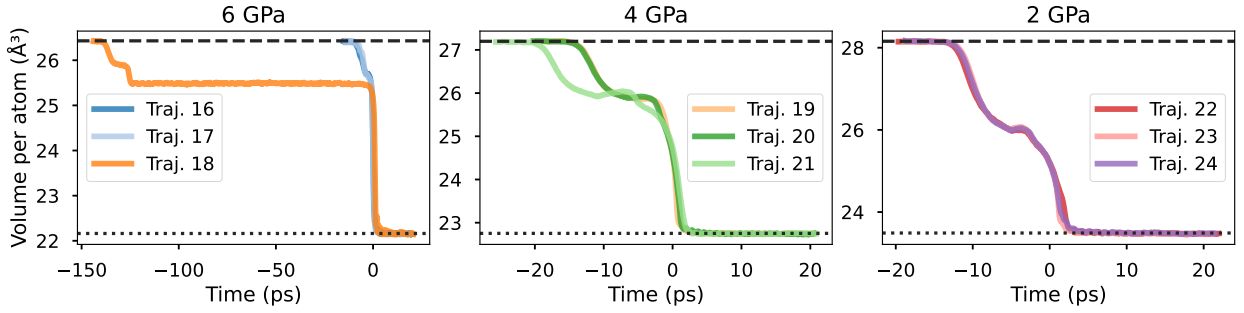

Figure S6 Comparison of volume per atom for for representative trajectories at 2, 4, and 6 GPa. The trajectories have been shifted in time so that the mean volume occurs at time 0. For each pressure we show three examples of representative trajectories, which have been numbered consecutively. The horizontal lines show the volume per atom for a wurtzite (dashed line) and a rock salt structure (dotted line) at the different pressures.

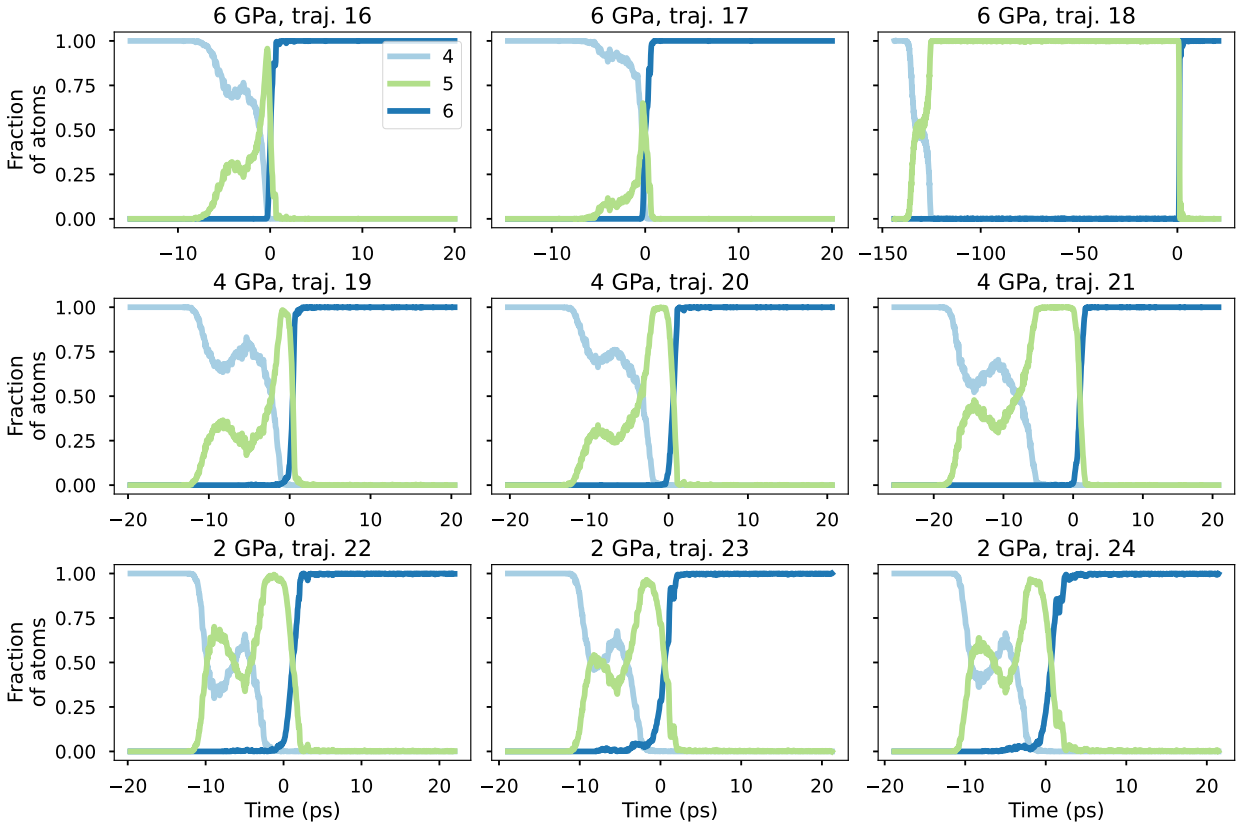

Figure S7 Fraction of atoms assigned as 4-, 5- or 6-coordinated for representative trajectories at 2, 4, and 6 GPa. These trajectories are the same as shown in figure S6, and the time has been shifted identically.

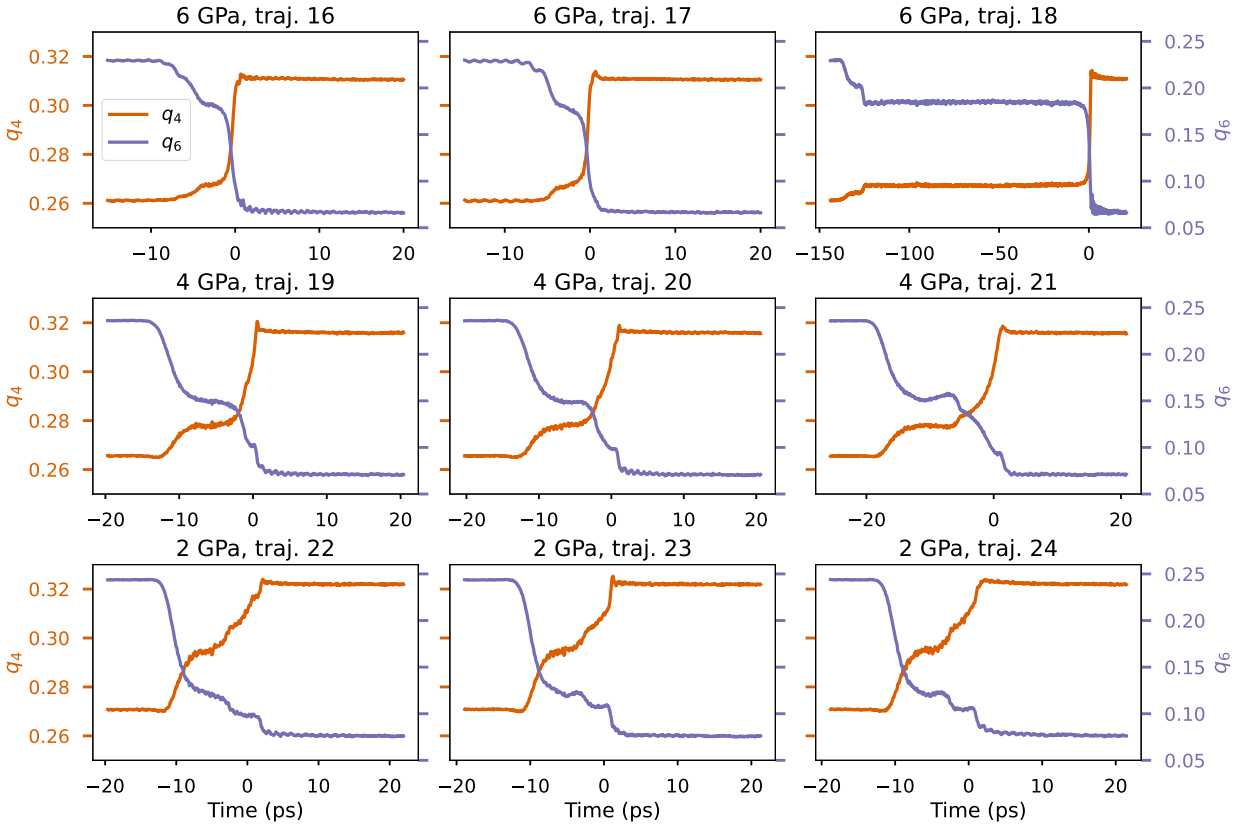

Figure S8 Mean Steinhardt order parameters of order 4 (q_4) and 6 (q_6) for representative trajectories at 2, 4, and 6 GPa. These trajectories are the same as shown in figure S6, and the time has been shifted identically.

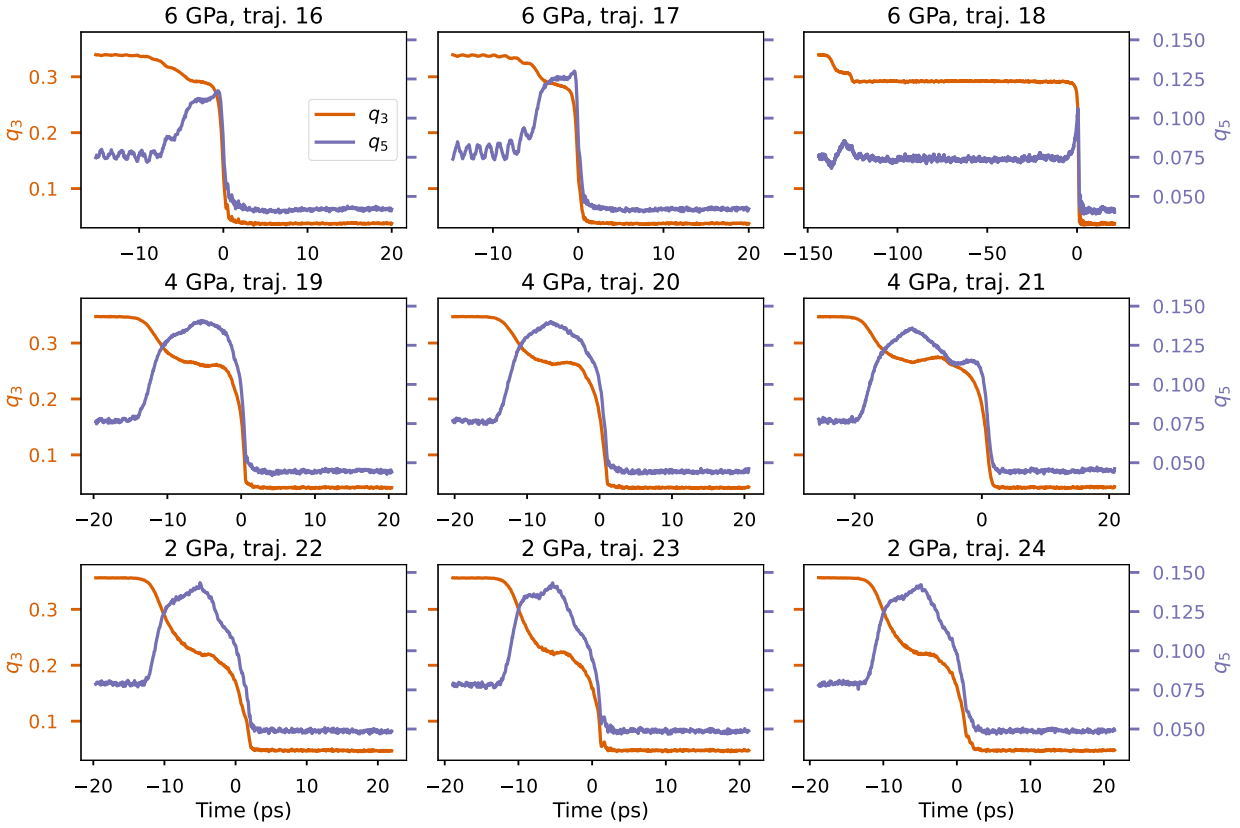

Figure S9 Mean Steinhardt order parameters of order 3 (q_3) and 5 (q_5) for representative trajectories at 2, 4, and 6 GPa. These trajectories are the same as shown in figure S6, and the time has been shifted identically.

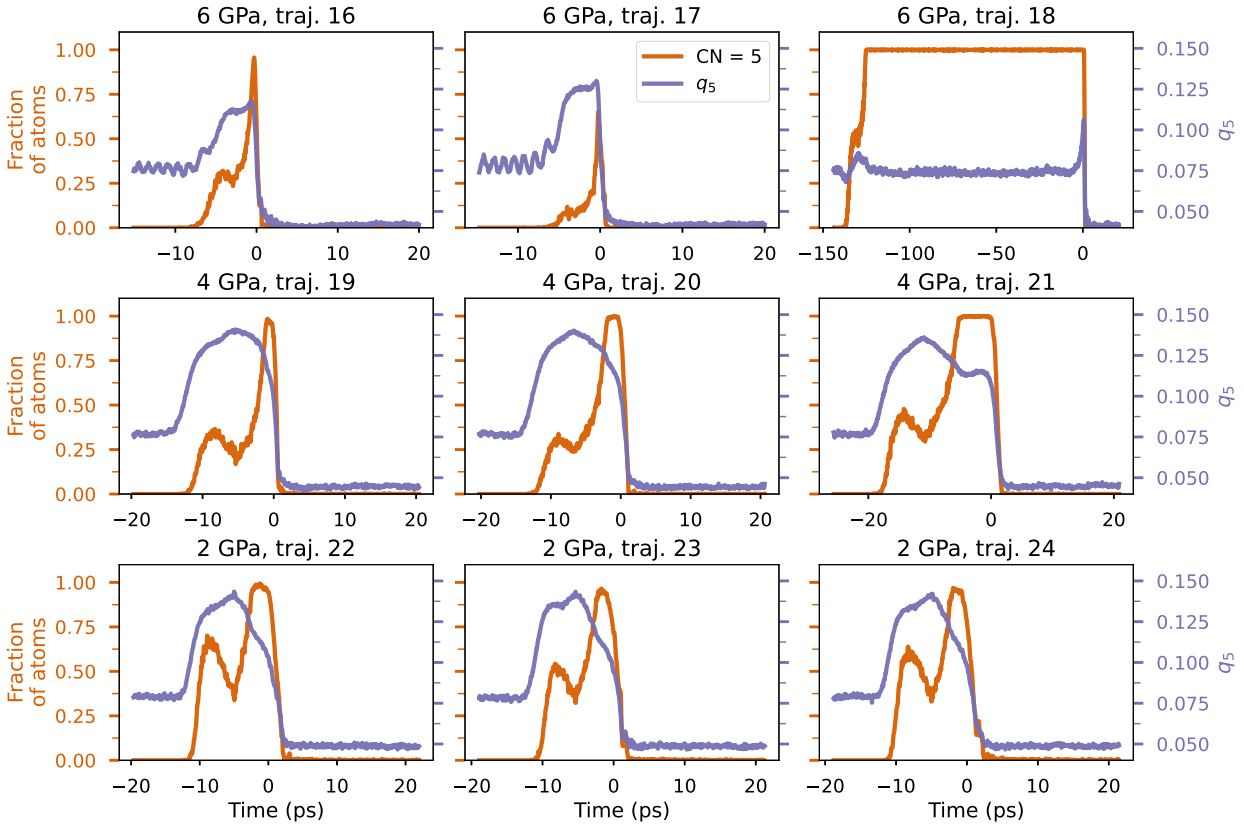

Figure S10 Fraction of atoms assigned as 5-coordinated ("CN = 5") and the mean Steinhardt order parameter of order 5 (q_5) for representative trajectories at 2, 4, and 6 GPa. These trajectories are the same as shown in figure S6, and the time has been shifted identically.

Additional results for systems with defects

Coordination numbers and Steinhardt order parameters are shown for cases with defects at 8 and 10 GPa in figures S11-S13 and for 6 GPa in figure S14. The results from the analysis of variance of the first passage times at 8 and 10 GPa with defects (16 Cd–Se pairs removed) are given in table S4.

Table S4 Analysis of variance for first passage times at 8 and 10 GPa for systems with 16 Cd–Se pairs removed.

Pressure (GPa)	Component	Sum of squares	Degrees of freedom	f-statistic	p-value
8	Between defect types	343.552196	1	70.862262	6×10^{-15}
	Within defect types	1008.419076	208		
10	Between defect types	25.029762	1	12.41937	5×10^{-4}
	Within defect types	419.199238	208		

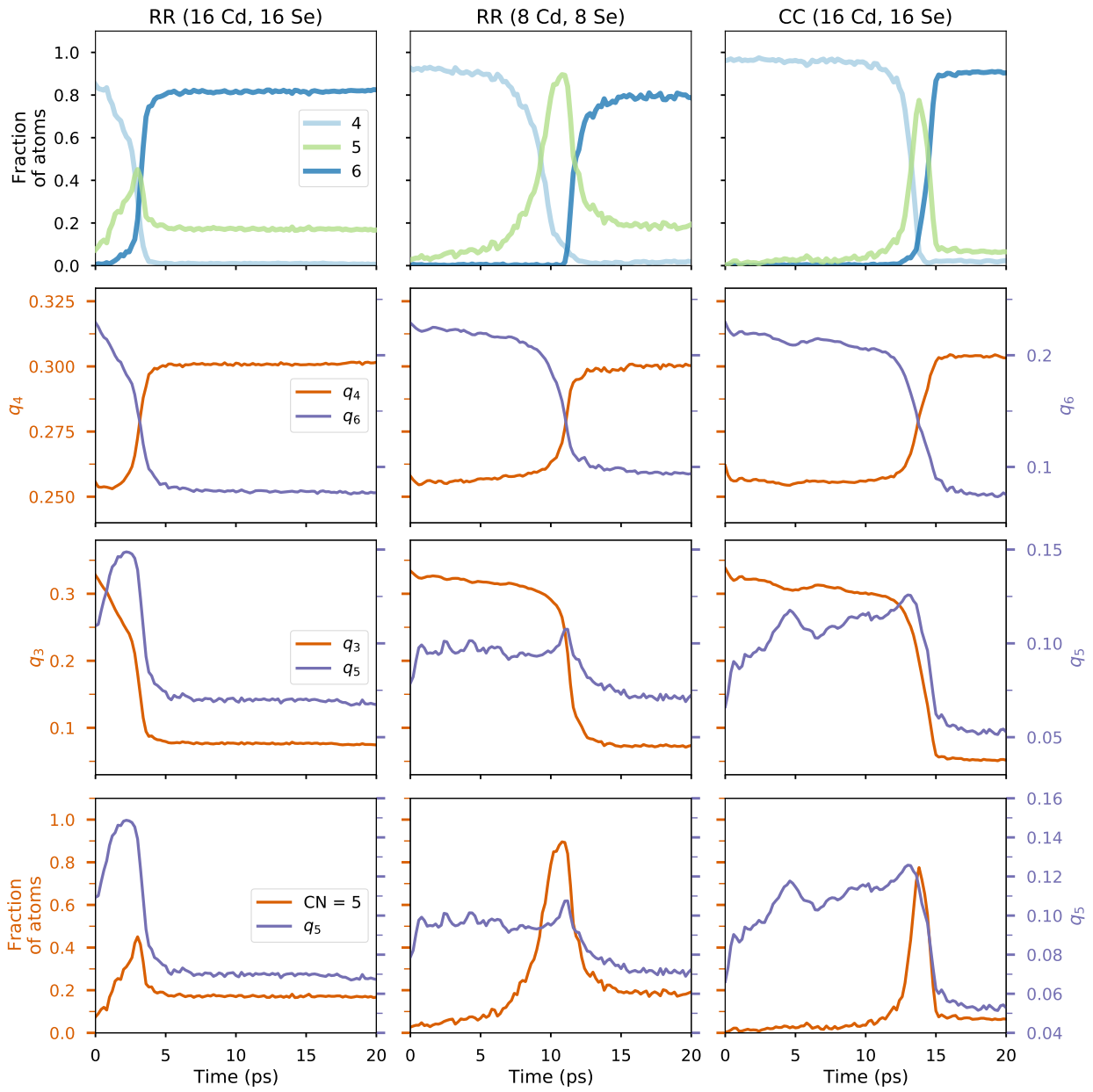

Figure S11 Fraction of atoms assigned as 4-, 5- or 6-coordinated, and mean Steinhardt order parameters of order 3 (q_3), 4 (q_4), 5 (q_5), and 6 (q_6) for 3 representative trajectories with defects at 8 GPa. The defects were created with the random removal approach ("RR") or cavity creation ("CC") as described in the main article. Here, we only show trajectories where the transition occurred. "CN = 5" refers to 5-coordinated atoms.

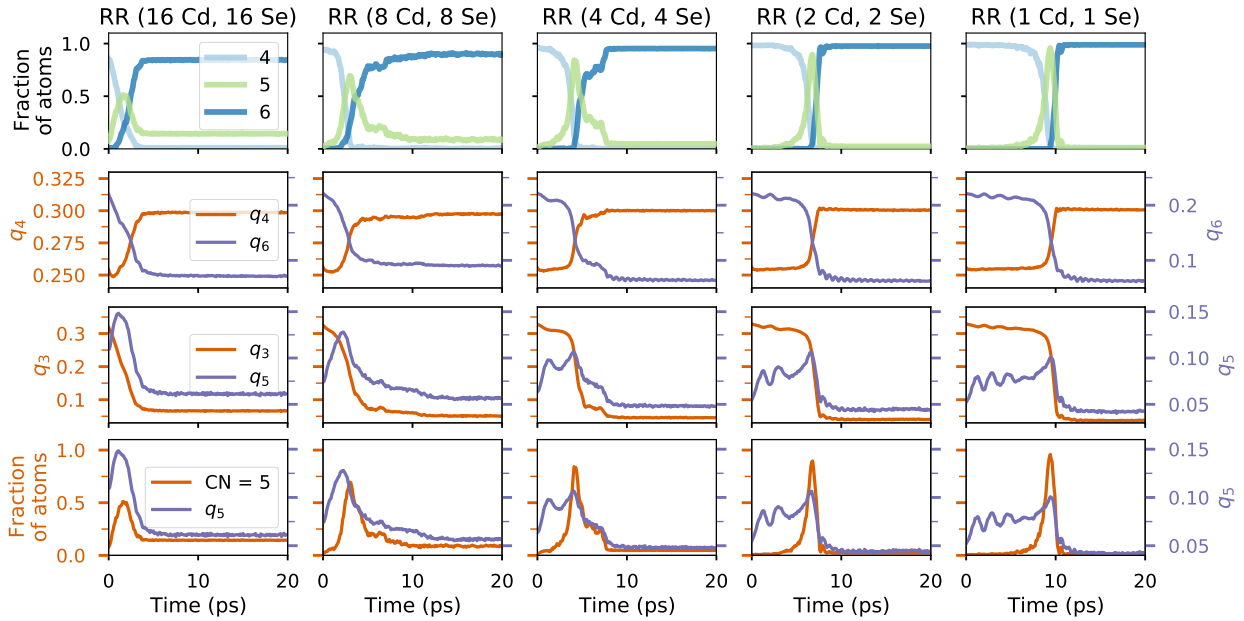

Figure S12 Fraction of atoms assigned as 4-, 5- or 6-coordinated, and mean Steinhardt order parameters of order 3 (q_3), 4 (q_4), 5 (q_5), and 6 (q_6) for 5 representative trajectories with defects at 10 GPa. The defects were created with the random removal approach ("RR") as described in the main article. "CN = 5" refers to 5-coordinated atoms.

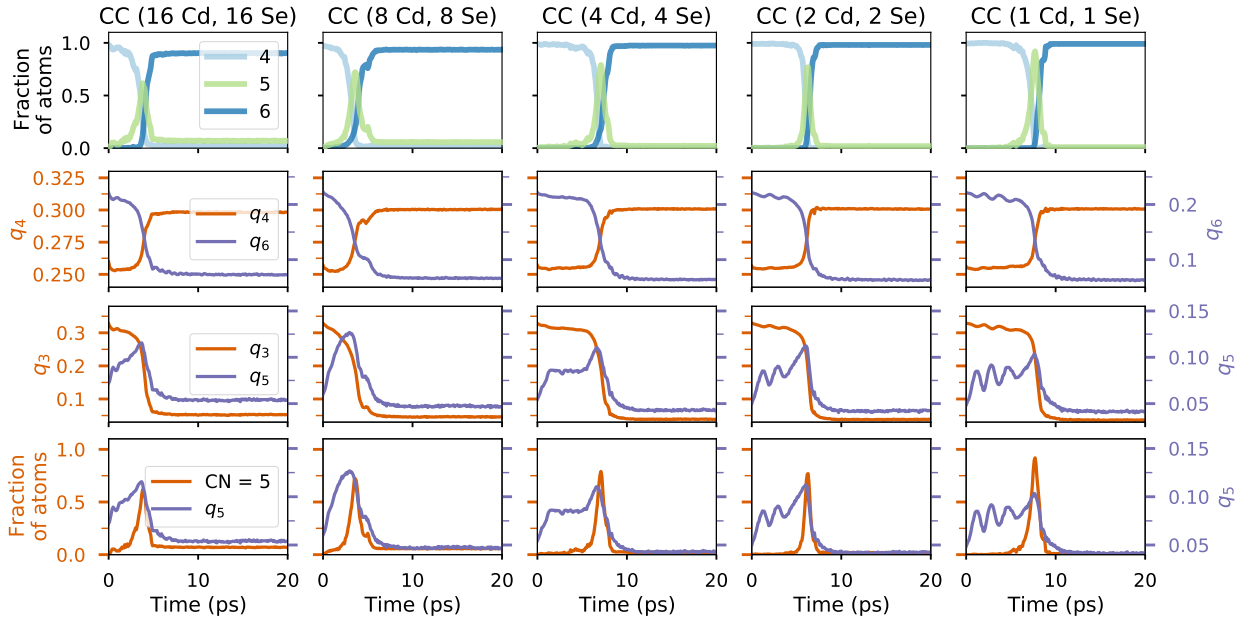

Figure S13 Fraction of atoms assigned as 4-, 5- or 6-coordinated, and mean Steinhardt order parameters of order 3 (q_3), 4 (q_4), 5 (q_5), and 6 (q_6) for 5 representative trajectories with defects at 10 GPa. The defects were created with the cavity creation approach ("CC") as described in the main article. "CN = 5" refers to 5-coordinated atoms.

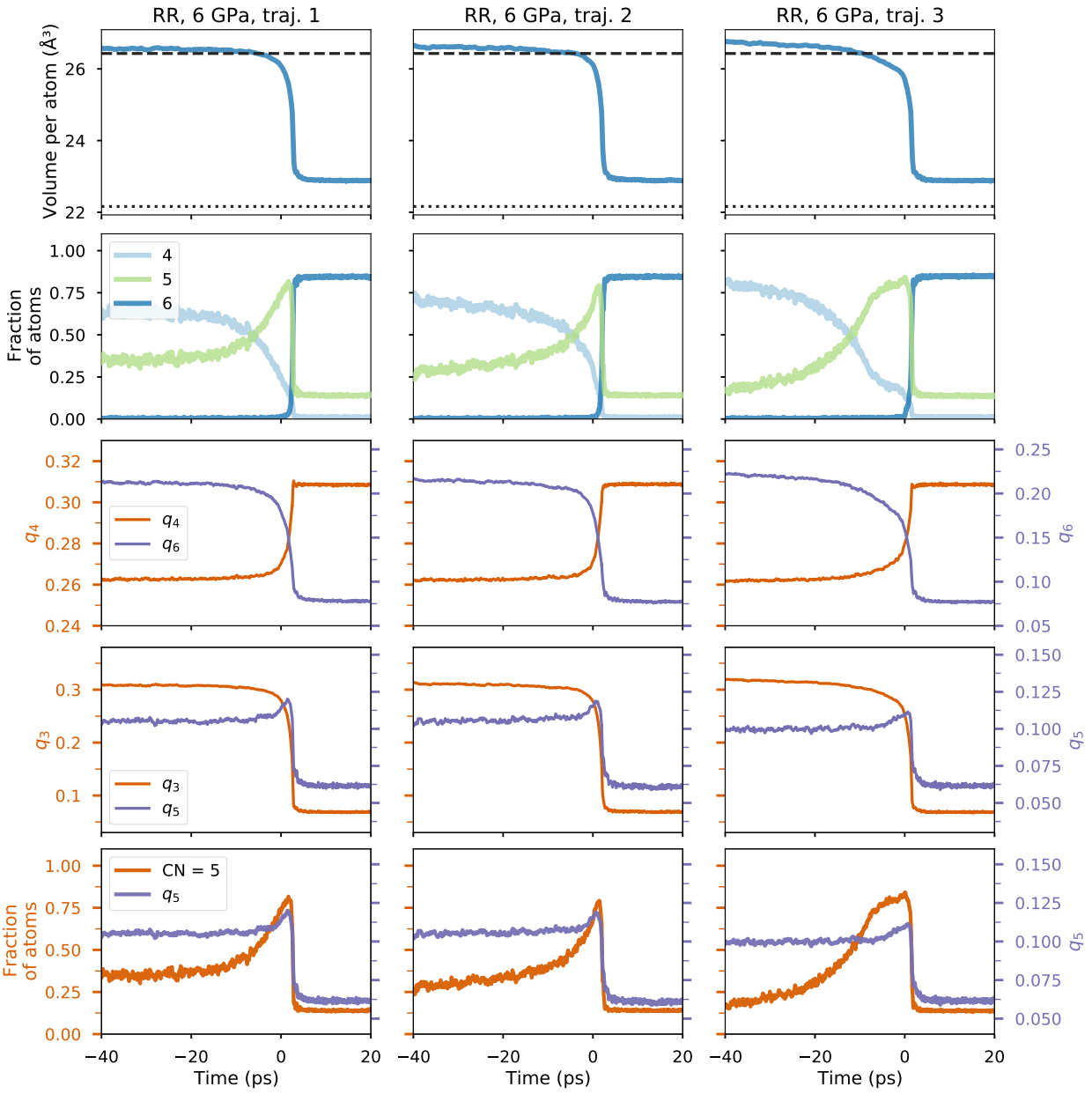

Figure S14 Fraction of atoms assigned as 4-, 5- or 6-coordinated, and mean Steinhardt order parameters of order 3 (q_3), 4 (q_4), 5 (q_5), and 6 (q_6) for 3 representative trajectories with defects at 6 GPa. The defects were created with the random removal approach ("RR") as described in the main article and 16 Cd and 16 Se atoms were removed. "CN = 5" refers to 5-coordinated atoms.

Analysis of change in box parameters

The change in the box parameters for trajectories from the RETIS simulations at different pressures are shown in figure S15 and S16. For the system with defects at 6 GPa, we show the change in the box parameters in figure S17.

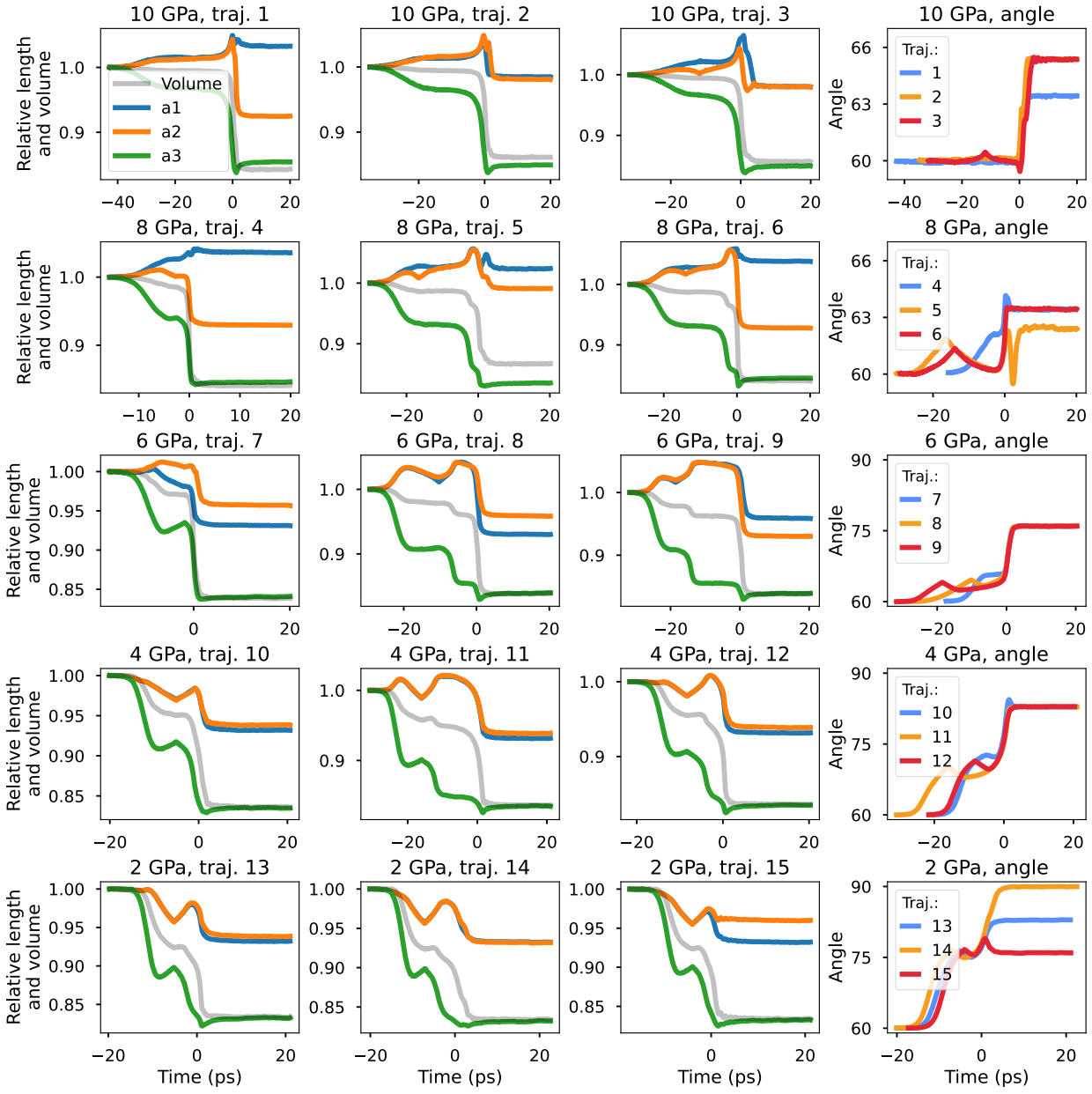

Figure S15 Box parameters as function of time for selected trajectories. These trajectories are the same as shown in figure 3 in the main article, and the time has been shifted identically. The box vector a1 is parallel to the x-axis, a2 is coplanar to x and a3 is parallel to the z-axis and normal to a1 and a2. The angle depicted in the last column is the angle between a1 and a2. The two other angles do not change significantly during the simulation (they remain approximately at 90°).

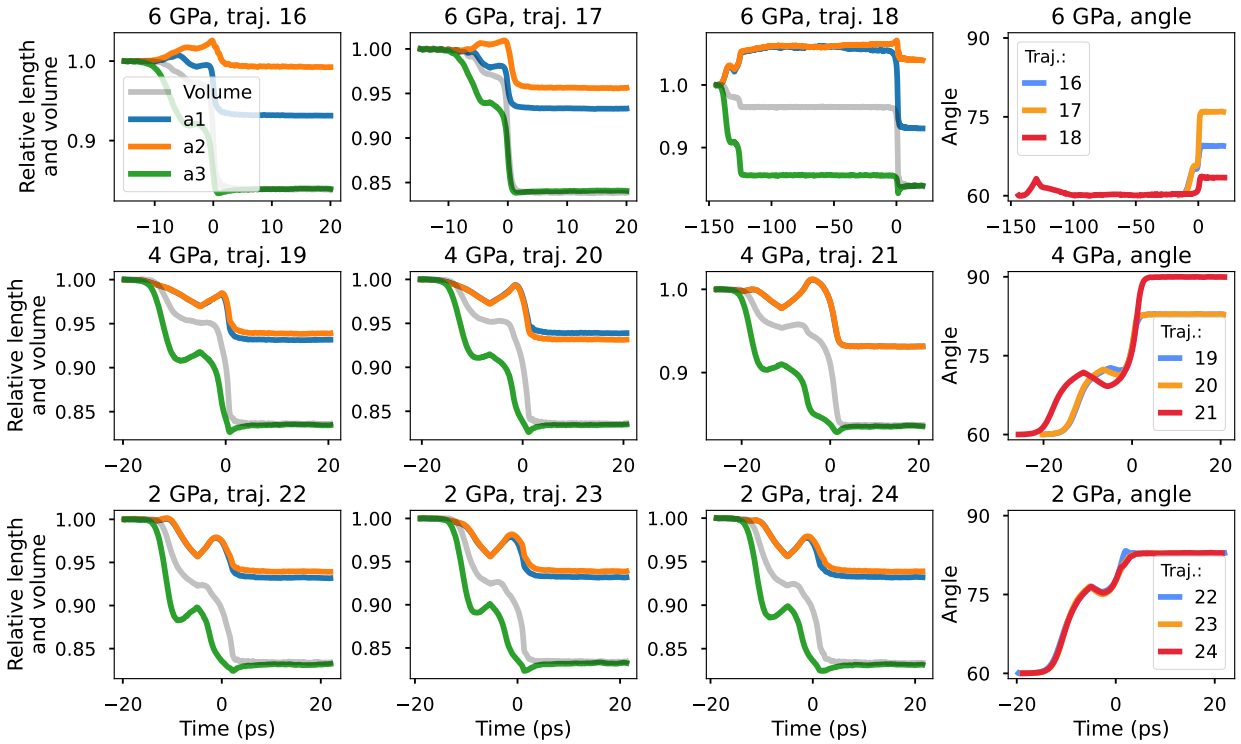

Figure S16 Box parameters as function of time for additional trajectories at 2, 4, and 6 GPa. These trajectories are the same as shown in figure S6, and the time has been shifted identically. The box vectors are labeled as described in figure S15.

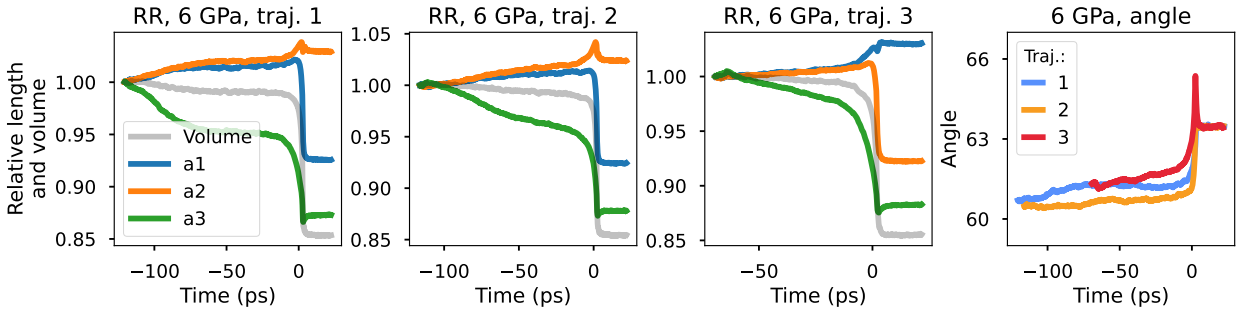

Figure S17 Box parameters as function of time for additional trajectories at 6 GPa. These trajectories are the same as shown in figure S14, and the time has been shifted identically. The box vectors are labeled as described in figure S15.

References

(1) Rabani, E. An interatomic pair potential for cadmium selenide. *J. Chem. Phys.* **2002**, *116*, 258–262, DOI: 10.1063/1.1424321.

(2) Kresse, G.; Furthmüller, J. Efficient iterative schemes for ab initio total-energy calculations using a plane-wave basis set. *Phys. Rev. B* **1996**, *54*, 11169–11186, DOI: 10.1103/PhysRevB.54.11169.

(3) Kresse, G.; Furthmüller, J. Efficiency of ab-initio total energy calculations for metals and semiconductors using a plane-wave basis set. *Computational Materials Science* **1996**, *6*, 15–50, DOI: https://doi.org/10.1016/0927-0256(96)00008-0.

(4) Jain, A.; Ong, S. P.; Hautier, G.; Chen, W.; Richards, W. D.; Dacek, S.; Cholia, S.; Gunter, D.; Skinner, D.; Ceder, G.; Persson, K. a. The Materials Project: A materials genome approach to accelerating materials innovation. *APL Materials* **2013**, *1*, 011002, DOI: 10.1063/1.4812323.

(5) Shimojo, F.; Kodiyalam, S.; Ebbsjö, I.; Kalia, R. K.; Nakano, A.; Vashishta, P. Atomistic mechanisms for wurtzite-to-rocksalt structural transformation in cadmium selenide under pressure. *Phys. Rev. B* **2004**, *70*, 184111, DOI: 10.1103/PhysRevB.70.184111.

(6) Perdew, J. P.; Burke, K.; Ernzerhof, M. Generalized Gradient Approximation Made Simple. *Phys. Rev. Lett.* **1997**, *78*, 1396–1396, DOI: 10.1103/PhysRevLett.78.1396.